Direct evidence of interaction-induced Dirac cones in a monolayer silicene/Ag(111) system

Ya Feng[a,1], Defa Liu[a,1], Baojie Feng[a,1], Xu Liu[a,1], Lin Zhao[a], Zhuojin Xie[a], Yan Liu[a], Aiji Liang[a], Cheng Hu[a], Yong Hu[a], Shaolong He[a], Guodong Liu[a], Jun Zhang[a], Chuangtian Chen[b], Zuyan Xu[b], Lan Chen[a], Kehui Wu[a,c], Yu-Tzu Liu[d,e], Hsin Lin[d,e], Zhi-Quan Huang[f], Chia-Hsiu Hsu[f], Feng-Chuan Chuang[f], Arun Bansil[g], and X. J. Zhou[a,c,h,2]

[a]Beijing National Laboratory for Condensed Matter Physics, Institute of Physics, Chinese Academy of Sciences, Beijing 100190, China; [b]Technical Institute of Physics and Chemistry, Chinese Academy of Sciences, Beijing 100190, China; [c]Collaborative Innovation Center of Quantum Matter, Beijing 100871, China; [d]Centre for Advanced 2D Materials and Graphene Research Centre, National University of Singapore, Singapore 117546; [e]Department of Physics, National University of Singapore, Singapore 117542; [f]Department of Physics, National Sun Yat-Sen University, Kaohsiung 804, Taiwan; [g]Department of Physics, Northeastern University, Boston, MA 02115; and [h]School of Physical Sciences, University of Chinese Academy of Sciences, Beijing 100190, China

Edited by Maw-Kuen Wu, Academia Sinica (Taiwan), Taipei, Taiwan, and approved November 11, 2016 (received for review August 11, 2016)

Silicene, analogous to graphene, is a one-atom-thick 2D crystal of silicon, which is expected to share many of the remarkable properties of graphene. The buckled honeycomb structure of silicene, along with enhanced spin-orbit coupling, endows silicene with considerable advantages over graphene in that the spin-split states in silicene are tunable with external fields. Although the low-energy Dirac cone states lie at the heart of all novel quantum phenomena in a pristine sheet of silicene, a hotly debated question is whether these key states can survive when silicene is grown or supported on a substrate. Here we report our direct observation of Dirac cones in monolayer silicene grown on a Ag(111) substrate. By performing angle-resolved photoemission measurements on silicene(3×3)/Ag(111), we reveal the presence of six pairs of Dirac cones located on the edges of the first Brillouin zone of Ag(111), which is in sharp contrast to the expected six Dirac cones centered at the K points of the primary silicene(1×1) Brillouin zone. Our analysis shows clearly that the unusual Dirac cone structure we have observed is not tied to pristine silicene alone but originates from the combined effects of silicene(3×3) and the Ag(111) substrate. Our study thus identifies the case of a unique type of Dirac cone generated through the interaction of two different constituents. The observation of Dirac cones in silicene/Ag(111) opens a unique materials platform for investigating unusual quantum phenomena and for applications based on 2D silicon systems.

photoemission | silicene | Dirac cone | interaction

Silicene is theoretically predicted to be stable in the honeycomb lattice and, like its cousin graphene, it harbors the characteristic low-energy Dirac cone states (1–6). Silicene can thus be expected to share many of the remarkable quantum properties of graphene (7–10). Distinct from graphene, however, which is dominated by sp^2 bonding and assumes an essentially flat structure, the crystal structure of silicene is naturally buckled as a result of the mixed sp^2/sp^3 bonding (2–5). The stronger spin-orbit coupling strength in silicene (11, 12) leads to a larger energy gap at the Dirac points, which would make it possible to access the quantum spin Hall effect experimentally at a higher temperature (11, 12). The buckled honeycomb structure drives a number of new phenomena and properties in silicene. In particular, the gap at the Dirac point can be tuned by applying external electric and magnetic fields to realize a variety of different phases and topological phase transitions (13–17). The unique advantages of silicene and its compatibility with the traditional silicon industry make it an attractive materials platform for next-generation nanoelectronics applications (18–23).

Single-layer and multilayer silicenes have been grown on various supporting materials, with the Ag(111) surface being the most common substrate (24–30). The buckled structure of silicene naturally leads to the formation of a variety of configurations beyond the primary (1×1) structure under different preparation conditions, such as the (3×3)/Ag(111) and ($\sqrt{3} \times \sqrt{3}$)R30°/Ag(111) structures (24–30). Although experimental signatures of Dirac cones have been reported in silicene, these results remain inconclusive (24, 31–38). For example, Vogt et al. (24) reported a "gapped Dirac cone" along the Γ–K direction near the K point in Ag(111), but only one side of the "Dirac cone" was observed, and it is not clear whether what was observed was the residual signal due to the Ag(111) substrate (24). Avila et al. (31) reported observation of a silicene-derived band with a clear gap and linear energy−momentum dispersion near the Fermi level at the Γ point of the (3×3) phase. Some groups have claimed that there are no Dirac cones but only saddle points in silicene (32, 33). Moreover, extensive theoretical work suggests that the interaction between silicene and the Ag(111) substrate will destroy the Dirac cones in silicene (38–43). The need for further experimental work to resolve these controversies is thus clear. Here we report direct observation of Dirac cones in monolayer silicene grown on Ag(111). By performing in-depth angle-resolved photoemission (ARPES) measurements on silicene(3×3)/Ag(111), we reveal the presence of six pairs of Dirac cones located on the edges of the

Significance

Silicene is a one-atom-thick 2D crystal of silicon. The low-energy Dirac cone states in silicene lie at the heart of all novel quantum phenomena and potential applications. However, so far, the evidence of Dirac cones in silicene is highly controversial. We report a direct observation of Dirac cones in monolayer silicene grown on a Ag(111) substrate. We further show that this unusual Dirac cone structure originates from the interaction of silicene with the Ag(111) substrate, establishing the case of a unique type of Dirac fermion generated through the interaction of two different constituents. The observation of Dirac cones in silicene(3×3)/Ag(111) opens a unique materials platform for investigating unusual quantum phenomena and for applications based on 2D silicon systems.

Author contributions: X.J.Z., Y.F., D.L., B.F., X.L., L.Z., Z. Xie, and K.W. proposed and designed the research; Y.F., D.L., B.F., X.L., L.Z., Z. Xie, L.C., and K.W. contributed in sample preparation; Y.F., D.L., X.L., L.Z., Z. Xie, Y.L., A.L., C.H., Y.H., S.H., G.L., J.Z., C.C., Z. Xu, and X.J.Z. contributed to the development and maintenance of Laser-ARPES system; Y.F., D.L., X.L., L.Z., and Z. Xie carried out the ARPES experiment; Y.F., D.L., B.F., X.L., L.Z., Z. Xie, and X.J.Z. analyzed the data; Y.-T.L., H.L., Z.-Q.H., C.-H.H., F.-C.C., and A.B. performed band structure calculations; and X.J.Z., Y.F., and A.B. wrote the paper with D.L., B.F., X.L., and L.Z., and all other authors contributed to writing the paper.

The authors declare no conflict of interest.

This article is a PNAS Direct Submission.

[1]Y.F., D.L., B.F., and X.L. contributed equally to this work.

[2]To whom correspondence should be addressed. Email: XJZhou@aphy.iphy.ac.cn.

This article contains supporting information online at www.pnas.org/lookup/suppl/doi:10.1073/pnas.1613434114/-/DCSupplemental.

first Brillouin zone (BZ) of Ag(111), not on the K points of the primary silicene(1 × 1) BZ. This result shows clearly that the observed Dirac cones originate not from the pristine silicene film alone but from the combined system of silicene(3 × 3) and the Ag(111) substrate. Our study thus identifies the case of a unique type of Dirac cone generated through the interaction of two different constituents. The existence of a unique form of Dirac cone pairs, beyond the usual Dirac cones expected near the K points in freestanding silicene, suggests that the silicene/Ag(111) system may possess unique phenomena and physical properties associated with its peculiar electronic structure. Our demonstration that silicene(3 × 3)/Ag(111) can harbor Dirac cones provides a pathway for exploiting 2D silicon system as materials platforms for investigating quantum phenomena and potential applications.

The silicene/Ag(111) sample was grown in situ in an ultrahigh vacuum chamber connected directly with an ARPES system. The Ag(111) single crystal was first cleaned via many cycles of Argon-ion sputtering and annealing at ∼800 K. Quality of the Ag(111) surface was checked by low-energy electron diffraction (LEED) and ARPES measurements on the surface state around the Γ point. Band structure of the Ag(111) surface was measured by ARPES for later comparison with the supported silicene surface. Silicene was grown by heating a piece of silicon wafer to directly deposit Si atoms on the preheated clean Ag(111) surface following the same procedure as described in ref. 27. The single-layer silicene(3 × 3)/Ag(111) sample was prepared at the Ag(111) substrate temperature of 470 K. Monolayer silicene(3 × 3)/Ag(111) was found to cover most of the surface area whereas other minor phases could be neglected as determined from the LEED patterns. Moreover, such a silicene(3 × 3) structure can exist only as the first layer on Ag(111); subsequent layers result in the formation of the $(\sqrt{3} \times \sqrt{3})$R30° phase (Fig. S1). We have repeated the growth process, followed by characterization of the film by LEED and a scanning tunneling microscope (STM) many times to make sure that the grown sample has a single-layer silicene(3 × 3) structure. The ARPES results on silicene(3 × 3)/Ag(111) presented in this study are highly reproducible. ARPES measurements were carried out in our laboratory system with a Scienta R4000 electron energy analyzer and a Helium discharge lamp, which provides a photon energy of 21.218 eV (44). The base pressure of the ARPES system is better than 5×10^{-11} Torr. The angular resolution is ∼0.3°and the energy resolution was set at 20 meV for increasing the measurement efficiency. The Fermi edge of a clean polycrystalline gold specimen connected to the sample was taken as the reference Fermi level. The deposition of potassium on the silicene/Ag(111) surface was realized by depositing it in situ for different times while keeping the sample at a low temperature of ∼20 K.

Fig. 1*A* shows a typical STM image of the monolayer silicene(3 × 3)/Ag(111) phase in which the 3 × 3 superstructure can be seen clearly (27). For convenient reference, Fig. 1*B* shows the first BZs of the Ag(111) surface and primary silicene(1 × 1), along with the folded BZ of silicene(3 × 3). Interestingly, the silicene(3 × 3) lattice has a good match with the Ag(111) surface because the first BZ of Ag(111) accommodates precisely 16 folded BZs of silicene(3 × 3). Fig. 1 *C1–C3* gives the constant energy contours of the clean Ag(111) surface at different binding energies. The Fermi surface (Fig. 1*C1*) is seen to consist of a clear electron pocket around the Γ point due to the well-known Shockley surface state (45) and a large hexagonal Fermi surface sheet along the Ag(111) BZ edge. As the binding energy

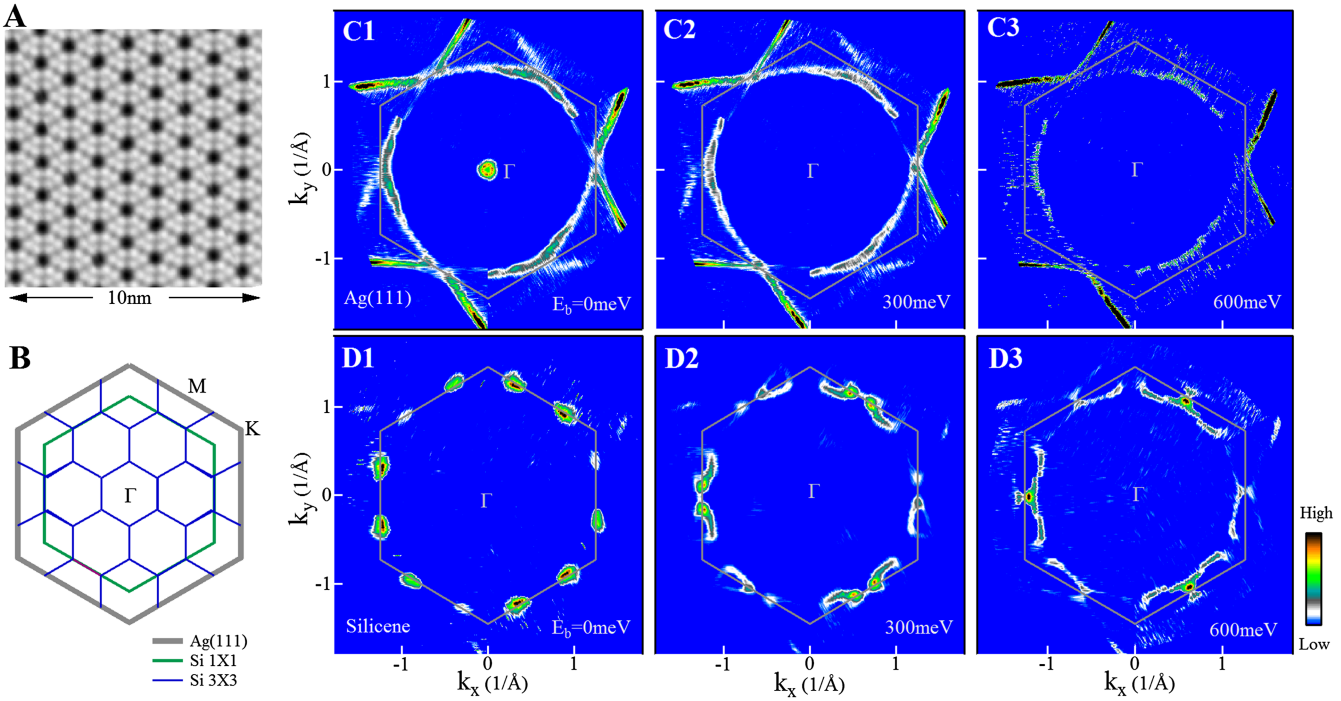

Fig. 1. Constant energy contours of silicene(3 × 3)/Ag(111) showing the existence of six pairs of Dirac cones. (*A*) STM image of silicene(3 × 3) grown on the Ag(111) surface. (*B*) First BZ of Ag(111) (thick gray solid line) and the corresponding BZs of silicene(1 × 1) (green line) and (3 × 3) supercell (thin blue line). Here silicene(3 × 3) is named with respect to the primary silicene(1 × 1) structure [it is named silicene (4 × 4) with reference to the Ag(111) surface]. (*C1–C3*) Constant energy contours of Ag(111) surface measured at 20 K obtained by integrating the photoemission spectral weight over a small energy window (±10 meV) with respect to the binding energy of 0 meV (*C1*), 300 meV (*C2*) and 600 meV (*C3*). (*D1–D3*) Constant energy contours of silicene(3 × 3)/Ag(111) measured at 20 K at three different binding energies of 0 meV (*D1*), 300 meV (*D2*) and 600 meV (*D3*). Some residual signal of the Ag(111) surface can be discerned, which is relatively stronger in the second BZ. In *C1–C3* and *D1–D3*, the gray line represents the first BZ of Ag(111) surface. The images are obtained by symmetrizing the original data, assuming threefold symmetry.

increases to 300 meV (Fig. 1*C2*) and 600 meV (Fig. 1*C3*), the central surface state disappears, whereas the bulk hexagonal contour keeps its basic shape but shows a slight decrease in area.

The Fermi surface of silicene(3 × 3)/Ag(111) (Fig. 1 *D1–D3*) shows interesting features that clearly set it apart from that of Ag(111) (Fig. 1 *C1–C3*). At monolayer silicene coverage, the signal of the Ag(111) surface-state pocket around Γ completely disappears, and that of the Ag(111) bulk states is strongly suppressed, although the residual signal is still discernable. These results are consistent with the single-layer growth mode of silicene(3 × 3) that can fully cover the Ag(111) surface. The Fermi surface topology of silicene(3 × 3)/Ag(111) exhibits 12 spots structure along the six edges of the Ag(111) first BZ (Fig. 1 *D1*). With increasing binding energy, these spots grow into approximately triangle-shaped pockets (Fig. 1 *D2* and *D3*). At high binding energies, the two pockets on the Ag(111) BZ edge touch and merge into each other (Fig. 1*D3*). Direct comparison of Fig. 1 *D1–D3* with the corresponding results for the Ag(111) surface (Fig. 1 *C1–C3*) as well as with the measured band structures (Fig. S2) indicates unambiguously that the observed Fermi pockets along the Ag(111) BZ edges must be associated with the silicene(3 × 3) structure grown on Ag(111). We show below (Figs. 2–4) that each strong spot here represents a Dirac cone structure in silicene(3 × 3)/Ag(111).

Fig. 2 clarifies details of how the observed Dirac cones evolve with increasing binding energy (Fig. S3). Two independent high-resolution ARPES measurements were carried out to simultaneously capture the Dirac cones around both the M (Fig. 2*A*) and the K (Fig. 2*B*) points. Similar to Fig. 1 *D1–D3*, with increasing binding energy, the constant energy contours for the two Dirac cones grow from spots at the Fermi level to triangle-shaped pockets with increasing area at higher binding energies. The constant energy contour lines at different binding energies are quantitatively shown in Fig. 2*C* for one of the Dirac cones; the results for the four different Dirac cones in Fig. 2*A* and *B* are consistent. These results indicate that the 12 Dirac cones observed around the Ag(111) BZ edges can be divided into 6 pairs, each of which is centered at the M point of the Ag(111) BZ edge, as shown schematically in Fig. 2*D*.

Fig. 3 shows the detailed band structure of silicene(3 × 3)/Ag(111) measured along different momentum cuts. For all of the momentum cuts across one Dirac cone (Fig. 3 *A–D*), two nearly linear bands extend over an energy range of 1 eV, consistent with our picture of the Dirac cones. In Fig. 3*A*, the two pairs of Dirac bands do not cross up to 1.4 eV, whereas in Fig. 3*B* along one Ag(111) BZ edge, the two pairs of Dirac cones intersect at ∼0.4 eV binding energy, consistent with the six-pair picture of Fig. 2*D*. In particular, Fig. 3*B* indicates that the observed signal is not simply a superposition of two individual Dirac cones, ruling out the possibility that one pair of Dirac cones on an edge comes from two domains with different orientations. This result is consistent with our LEED results where there is only a 3 × 3

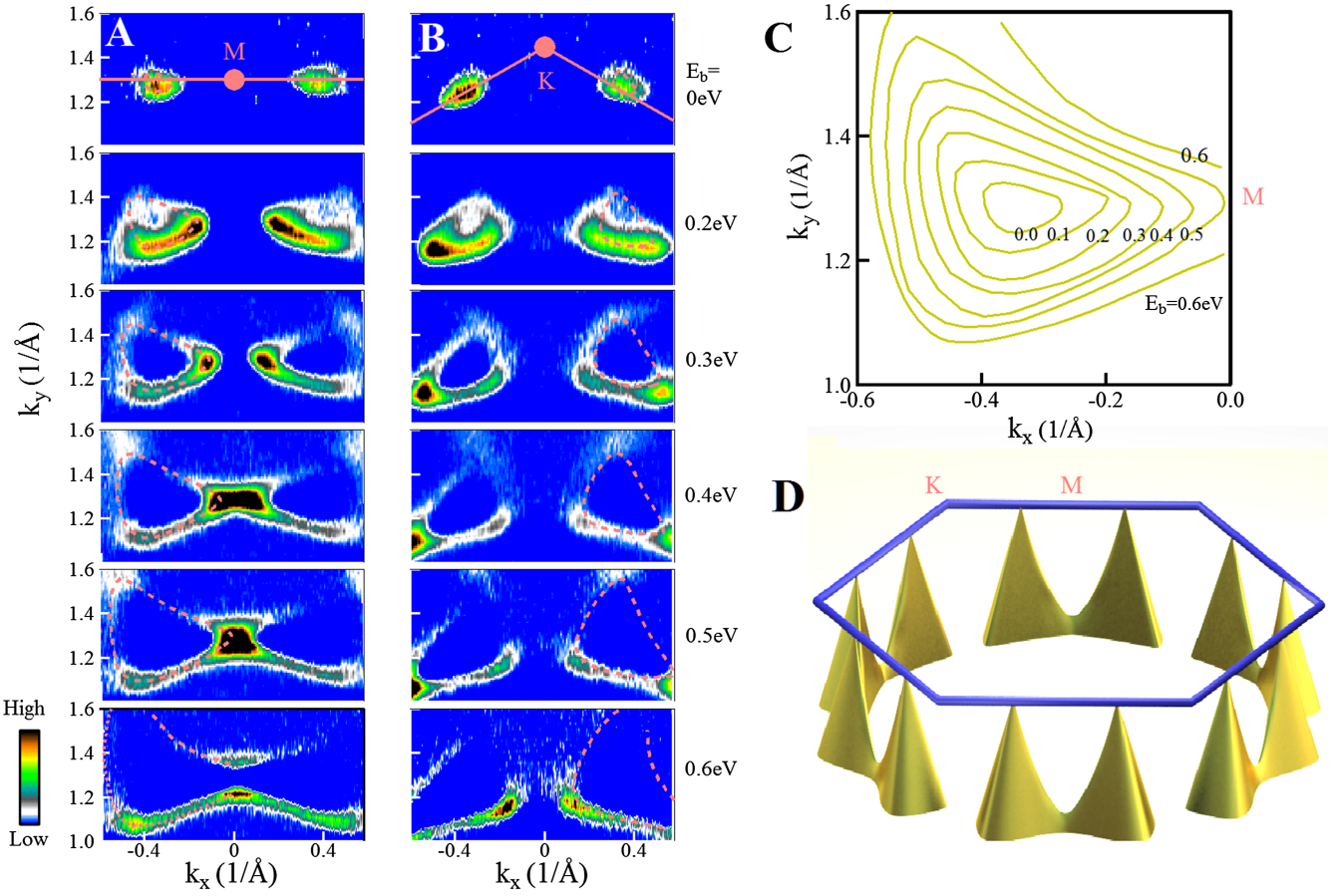

Fig. 2. Evolution of the Dirac cones in silicene(3 × 3)/Ag(111) with binding energy. (*A*) Constant energy contours of one pair of Dirac cones around the M point obtained by integrating the photoemission spectral weight over a small energy window (±10 meV) for binding energies of 0 meV, 200 meV, 300 meV, 400 meV, 500 meV, and 600 meV (from *Top* to *Bottom*). (*B*) Constant energy contours of two Dirac cones around the K point at different binding energies. (*C*) Constant energy contours of a single Dirac cone obtained by the contour lines at different binding energies of 0 meV, 200 meV, 300 meV, 400 meV, 500 meV, and 600 meV (dashed orange lines in *A* and *B*). (*D*) Schematic 3D diagram showing the existence of 12 Dirac cones in silicene(3 × 3)/Ag(111) forming 6 pairs along the first BZ edges of the Ag(111) surface (thick blue line).

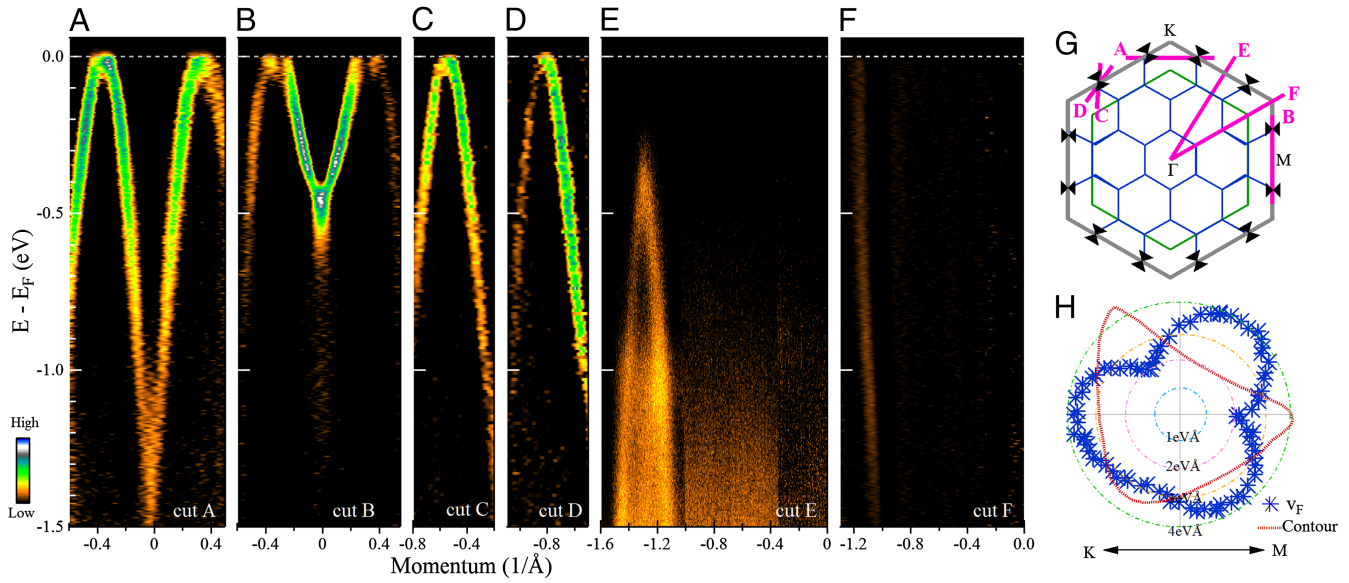

Fig. 3. Band structures of silicene(3 × 3)/Ag(111) along different momentum cuts. (*A*–*F*) Band structures measured along six typical momentum cuts. Location of the six momentum cuts is shown in *G*. To highlight the measured bands, the images shown are second-derivative images of the original data with respect to the momentum. Note that the faint band in *F* for the cut *F* is from the residual signal of Ag(111) bulk band as can be seen from the Ag(111) band structure (Fig. S2*C*). (*H*) Fermi velocity of the Dirac cone along different directions plotted as blue asterisks in a polar coordinate. The triangle-shaped brown line represents the corresponding constant-energy contour line of the Dirac cone at a binding energy of 0.5 eV (Fig. 2*C*).

superstructure along a single orientation (Fig. S1). For a given Dirac cone, different cuts give similar linear bands but with different dispersions (Fig. 3 *C* and *D*). Fig. 3*H* plots the Fermi velocity of one Dirac cone along different orientations; the values are obtained by fitting the bands near the Fermi level along different momentum cuts (Figs. 2 *A*–*C* and 3 *A*–*D*). It is clear that the Dirac cone in silicene(3 × 3)/Ag(111) is actually not cone-like in that its cross-section at various binding energies is more like a triangle than a circle (Figs. 2 and 3*H*). The resulting Fermi velocity is quite anisotropic with an approximate threefold symmetry, varying from 2 eV to 4 eV·Å(corresponding to 3–6 × 10^5 m/s) (Fig. 3*H*). Notably, no Fermi crossing is seen on the measured band in Fig. 3*E*, consistent with the six pairs of Dirac cones picture schematically shown in Fig. 2*D*.

It is clear that the Dirac points of our silicene(3 × 3)/Ag(111) sample lie above the Fermi level and therefore cannot be seen at low temperatures because of the Fermi–Dirac cutoff of the photoemission process. To observe the upper Dirac branch and thus the whole Dirac cone, we have used two different approaches. The first one is to warm up the sample to make use of thermal excitation of electrons above the Fermi level (Fig. 4 *A*–*D*). Dividing out the corresponding Fermi–Dirac distribution function makes it possible to observe a portion of the band structure above the Fermi level at high temperature. As seen

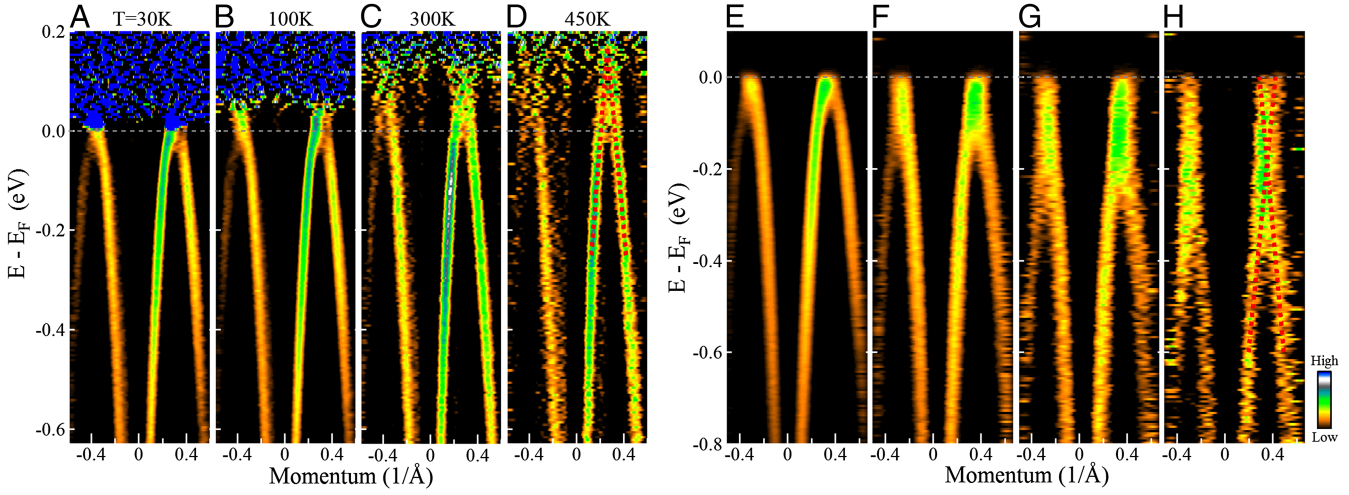

Fig. 4. Revelation of the Dirac cone and the upper Dirac branch in silicene(3 × 3)/Ag(111). (*A*–*D*) Band structures measured along the cut *A* in Fig. 3*G* at a temperature of 30 K (*A*), 100 K (*B*), 300 K (*C*), and 450 K (*D*). The images have been divided by the corresponding Fermi–Dirac distribution functions to observe band structures above the Fermi level. (*E*–*H*) Band structures measured along the cut *A* in Fig. 3*G* after depositing potassium on the surface. When an increasing amount of potassium is deposited on the sample surface, the overall band structure shifts to higher binding energy because of electron doping. The red dashed lines in *D* and *H* are guides to the eye through the observed bands.

in Fig. 4*D*, the Dirac bands are stable up to 450 K. Also the Dirac cone is observable at 450 K, which is about 170 meV above the Fermi level (Fig. 4*D*). These results indicate that our silicene(3 × 3)/Ag(111) sample is hole doped. An alternative way to reveal the Dirac point and the upper Dirac branch is to deposit potassium onto the silicene(3 × 3)/Ag(111) surface, which is expected to provide electron doping. As seen in Fig. 4 *E*–*H*, with increasing potassium deposition, indeed the Dirac cone shifts downward as expected. When the potassium doping is high enough (Fig. 4*H*), the Dirac cone is shifted to nearly 200 meV below the Fermi level and the upper Dirac bands become visible. In this case, the sample has become electron doped. These results further establish the Dirac cone structure in the silicene(3 × 3)/Ag(111) sample and demonstrate the possibility of transforming the sample from being hole doped to electron doped. We note that, when the bands are shifted down by sufficient potassium deposition, there appears a vertical straight intensity section in the observed bands (Fig. 4 *F*–*H*). A similar phenomenon has also been seen in graphene that is a well-known Dirac system (46). It was proposed to be due to band-gap opening although its origin is unclear (46, 47). Such a straight intensity section can also be produced by a two-band crossing combined with the effects of spectral broadening.

There have been a number of previous ARPES studies of silicene(3 × 3)/Ag(111) (24, 31–33), but we are not aware of any previous report of the presence of the six-pair Dirac cone structure that we have observed here. We emphasize that high sample quality and high-resolution ARPES measurements with a large and fine momentum coverage both play a crucial role in allowing us to reveal such a Dirac cone structure in silicene(3 × 3)/Ag(111). By high sample quality we mean that the monolayer silicene(3 × 3) covers nearly the entire Ag(111) surface, with little extra silicene on top of the silicene(3 × 3) layer to form other silicene superstructures. This leads to the maximum silicene(3 × 3)-related signal, the strongly suppressed residual Ag(111) signal, and a much-reduced signal and complications from other silicene superstructures. Our study provides a unified picture that helps resolve controversies related to the earlier ARPES results on silicene(3 × 3)/Ag(111) as follows. As we have pointed out already, Vogt et al. (24) reported observation of a gapped Dirac cone along the Γ–K direction near the K point in silicene(3 × 3)/Ag(111) (24), but raised a number of questions. First, for the pure Ag(111) surface, little signal was observed unlike the strong signals observed in ours (Fig. S2*C*) as well as previous ARPES measurements (31–33). Second, the purported Dirac cone showed only one side of bands with the signal near the Fermi level smeared out (24). In contrast, in our results, it is clear that there is no Dirac cone structure near the K point. The weak band reported by Vogt et al. (24) is likely due to the residual signal from Ag(111), as seen also in our Fig. S2*A*. In another earlier study, Avila et al. (31) reported observation of silicene-derived bands with a clear gap and a linear energy−momentum dispersion near the Fermi level at the Γ point of the (3 × 3) phase in several distinct BZs, consistent with our findings (Fig. 3*E*); what Avila et al. observed is not a gapped Dirac cone, but a saddle point near the M point formed by the Dirac cone pair along the Ag(111) BZ edge. Finally, Tsoutsou et al. (32) reported observation of a saddle point near the M point in silicene(3 × 3)/Ag(111); similar results were also reported by Mahatha et al. (33). Their conclusion of the M point being a saddle point is in accord with our results even though they did not reveal the presence of six pairs of Dirac cones in silicene(3 × 3)/Ag(111) because their silicene(3 × 3) signal presumably was not distinguished sufficiently from that of the residual Ag(111) and other silicene-related superstructures.

Now we discuss the origin of the six-pair Dirac cone structure we have observed in monolayer silicene(3 × 3)/Ag(111). One may wonder whether our observed electronic features might come from Ag(111) due to changes in the work function of Ag(111) upon silicene deposition. This possibility can be unambiguously ruled out by examining the constant energy contours in Fig. 1, which for those of Ag(111) (Fig. 1 *C1*–*C3*) are seen to be dramatically different from those of silicene(3 × 3)/Ag(111) (Fig. 1 *D1*–*D3*) over a large energy range (∼600 meV in Fig. 1). It is clear that a simple energy shift cannot produce the constant energy contours from Ag(111) (Fig. 1 *C1*–*C3*) that would resemble those in silicene(3 × 3)/Ag(111) (Fig. 1 *D1*–*D3*). Another possibility is that the observed six-pair Dirac cone structure in silicene(3 × 3)/Ag(111) comes from Ag(111) due to the presence of two domains rotated with respect to each other by 60°. This possibility, however, can also be completely ruled out for the following reasons: (*i*) There is no evidence of the existence of two domains on Ag(111) from our LEED and ARPES measurements as the constant energy contours in Fig. 1 *C1*–*C3* show threefold symmetry; (*ii*) as shown in Fig. 1, if we superpose the original constant energy contours of Ag(111) (Fig. 1 *C1*–*C3*) with the same spectra rotated by 60°, the resulting constant energy contours do not look anything like those of silicene(3 × 3)/Ag(111) shown in Fig. 1 *D1*–*D3*; and (*iii*) as Fig. 3*B* shows, for the cut along the Ag(111) BZ edge, there is a band bottom at the M point that is nearly 0.45 eV below the Fermi level. If the two Dirac cones were to come from two rotated domains, we would expect a superposition of two sets of Dirac bands at the M point, which is not consistent with our observation of a single parabolic band near M. The preceding arguments are conclusive in ruling out the presence of two rotated domains as the possible cause for our six-pair Dirac cone structure.

We emphasize that our observation of six pairs of Dirac cones in silicene(3 × 3)/Ag(111) is unusual for a number of reasons as follows. First, the present Dirac cones are fundamentally different from the commonly discussed Dirac cones that lie at the K points for a freestanding silicene honeycomb lattice. In sharp contrast, the present six pairs of Dirac cones lie on the edges of the first BZ of Ag(111) without any obvious connection with the BZ of silicene(1 × 1). Second, although the (3 × 3) superstructure of silicene could be expected to induce band-folding features (Fig. 1*B*), we do not observe such features in our spectra. We thus conclude that the six-pair Dirac cone structure we have observed in silicene(3 × 3)/Ag(111) does not exist in either freestanding silicene(3 × 3) or the Ag(111) surface alone and that it is generated through the interaction between the pristine silicene film and the Ag(111) substrate when the two systems are combined. Note that the low-energy electronic states in silicene(3 × 3)/Ag(111) will be formed through the hybridization of silicene and Ag(111) sp states with their periodicity dictated essentially by the Ag(111) lattice. Interestingly, the observed Dirac cones are situated near the intersection of the corners of the reduced silicene (3 × 3) BZ and the edges of the Ag(111) BZ, which is consistent with the notion that these Dirac cones arise via interaction between silicene and the Ag(111) substrate. This result is also in line with theoretical predictions (38–43) and experimental measurements (32, 33), which indicates that the Ag(111) substrate interacts strongly with silicene and destroys the Dirac cones at the K points of freestanding silicene(1 × 1) (38–43).

In this connection, we have carried out extensive first-principles modeling of the electronic structure of silicene/Ag(111) systems (Fig. S4). However, our own computations, as well as the large number of those available in the literature (38–43), do not explain our observed Dirac cone structure. This is surprising because we do not expect strong correlation effects to be at play here, so that the band theory framework should provide a reasonable description of the electronic states. Failure of the existing calculations to account for our observations suggests that the structural models of the silicene/Ag(111) interface used so far

may not be adequate and that alternative models involving consideration of defects, reconstructions, and reactions (48) should be investigated.

In summary, we have provided direct evidence for the existence of six pairs of Dirac cones in the monolayer silicene(3×3)/Ag(111) system. We have demonstrated that this unusual Dirac cone structure comes into existence only when the silicene film is grown on the Ag(111) substrate. Our study thus identifies a unique type of Dirac cone structure, which is obtained through the interaction of silicene with the substrate to generate a state that is distinct from that of the individual constituents. The observed six-pair Dirac cone structure in the silicene/Ag(111) system cannot be understood in terms of the existing band structure calculations, and we hope that our study will stimulate further related theoretical work. Our observation of a unique Dirac cone structure in silicene(3×3)/Ag(111), and the possibility of hole or electron doping of these Dirac cones, opens a unique materials pathway for fundamental science investigations and applications based on 2D silicon systems.

ACKNOWLEDGMENTS. X.J.Z. received financial support from the National Science Foundation of China (Grants 91021006 and 11474336), the Ministry of Science and Technology (MOST) of China (973 Program nos. 2012CB821402, 2013CB921700, and 2013CB921904), and the Strategic Priority Research Program (B) of the Chinese Academy of Sciences (Grant XDB07020300). The work at Northeastern University was supported by the US Department of Energy (DOE), Office of Science, Basic Energy Sciences Grant DE-FG02-07ER46352 (core research), and benefited from Northeastern University's Advanced Scientific Computation Center, the NERSC supercomputing center through DOE Grant DE-AC02-05CH11231, and support (applications to layered materials) from the DOE Energy Frontier Research Centers: Center for the Computational Design of Functional Layered Materials under Grant DE-SC0012575. H.L. acknowledges the Singapore National Research Foundation for support under National Research Foundation (NRF) Award NRF-NRFF2013-03. F.-C.C. acknowledges support from the National Center for Theoretical Sciences and the Taiwan Ministry of Science and Technology under Grants MOST-101-2112-M-110-002-MY3 and MOST-101-2218-E-110-003-MY3 and the support the National Center for High Performance Computing for computer time and facilities.

1. Bansil A, Lin H, Das T (2016) *Colloquium*: Topological band theory. *Rev Mod Phys* 88:021004.
2. Takeda K, Shiraishi K (1994) Theoretical possibility of stage corrugation in Si and Ge analogs of graphite. *Phys Rev B Condens Matter* 50:14916–14922.
3. Guzman-Verri GG, Lew Yan Voon LC (2007) Electronic structure of silicon-based nanostructures. *Phys Rev B* 76:075131.
4. Cahangirov S, Topsakal M, Aktürk E, Sahin H, Ciraci S (2009) Two- and one-dimensional honeycomb structures of silicon and germanium. *Phys Rev Lett* 102: 236804.
5. Lebegue S, Eriksson O (2009) Electronic structure of two-dimensional crystals from ab initio theory. *Phys Rev B* 79:115409.
6. Lew Yan Voon LC, Sandberg E, Aga RS, Farajian AA (2010) Hydrogen compounds of group-IV nanosheets. *Appl Phys Lett* 97:163114.
7. Novoselov KS, et al. (2004) Electric field effect in atomically thin carbon films. *Science* 306:666–669.
8. Novoselov KS, et al. (2005) Two-dimensional gas of massless Dirac fermions in graphene. *Nature* 438:197–200.
9. Zhang Y, Tan YW, Stormer HL, Kim P (2005) Experimental observation of the quantum Hall effect and Berry's phase in graphene. *Nature* 438:201–204.
10. Castro Neto AH, Guinea F, Peres NMR, Novoselov KS, Geim AK (2009) The electronic properties of graphene. *Rev Mod Phys* 81:109–162.
11. Liu CC, Feng W, Yao Y (2011) Quantum spin Hall effect in silicene and two-dimensional germanium. *Phys Rev Lett* 107:076802.
12. Liu CC, Jiang H, Yao Y (2011) Low-energy effective Hamiltonian involving spin-orbit coupling in silicene and two-dimensional germanium and tin. *Phys Rev B* 84:195430.
13. Ni Z, et al. (2012) Tunable bandgap in silicene and germanene. *Nano Lett* 12:113–118.
14. Drummond ND, Zólyomi V, Fal'ko VI (2012) Electrically tunable band gap in silicene. *Phys Rev B* 85:075423.
15. Ezawa M (2012) A topological insulator and helical zero mode in silicene under an inhomogeneous electric field. *New J Phys* 14:033003.
16. Ezawa M (2012) Valley-polarized metals and quantum anomalous Hall effect in silicene. *Phys Rev Lett* 109:055502.
17. Stille L, Tabert CJ, Nicol EJ (2012) Optical signatures of the tunable band gap and valley-spin coupling in silicene. *Phys Rev B* 86:195405.
18. Kara A, et al. (2012) A review on silicene — new candidate for electronics. *Surf Sci Rep* 67:1–18.
19. Tsai WF, et al. (2013) Gated silicene as a tunable source of nearly 100% spin-polarized electrons. *Nat Commun* 4:1500.
20. An X-T, Zhang Y-Y, Liu J-J, Li S-S (2012) Spin-polarized current induced by a local exchange field in a silicene nanoribbon. *New J Phys* 14:083039.
21. Liu F, Liu CC, Wu K, Yang F, Yao Y (2013) d + id' chiral superconductivity in bilayer silicene. *Phys Rev Lett* 111:066804.
22. Kikutake K, Ezawa M, Nagaosa N (2013) Edge states in silicene nanodisks. *Phys Rev B* 88:115432.
23. Linder J, Yokoyama T (2014) Superconducting proximity effect in silicene: Spin-valley-polarized Andreev reflection, nonlocal transport, and supercurrent. *Phys Rev B* 89:020504(R).
24. Vogt P, et al. (2012) Silicene: Compelling experimental evidence for graphenelike two-dimensional silicon. *Phys Rev Lett* 108:155501.
25. Lin C-L, et al. (2012) Structure of silicene grown on Ag(111). *APEX* 5:045802.
26. Fleurence A, et al. (2012) Experimental evidence for epitaxial silicene on diboride thin films. *Phys Rev Lett* 108:245501.
27. Feng B, et al. (2012) Evidence of silicene in honeycomb structures of silicon on Ag(111). *Nano Lett* 12:3507–3511.
28. Jamgotchian H, et al. (2012) Growth of silicene layers on Ag(111): Unexpected effect of the substrate temperature. *J Phys Condens Matter* 24:172001.
29. Meng L, et al. (2013) Buckled silicene formation on Ir(111). *Nano Lett* 13:685–690.
30. Jamgotchian H, et al. (2014) A comprehensive study of the $(2\sqrt{3} \times 2\sqrt{3})$R30° structure of silicene on Ag(111). arXiv:1412.4902.
31. Avila J, et al. (2013) Presence of gapped silicene-derived band in the prototypical (3×3) silicene phase on silver (111) surfaces. *J Phys Condens Matter* 25:262001.
32. Tsoutsou D, Xenogiannopoulou E, Golias E, Tsipas P, Dimoulas A (2013) Evidence for hybrid surface metallic band in (4×4) silicene on Ag(111). *Appl Phys Lett* 103: 231604.
33. Mahatha SK, et al. (2014) Silicene on Ag(111): A honeycomb lattice without Dirac bands. *Phys Rev B* 89:201416(R).
34. De Padova P, et al. (2013) Evidence of Dirac fermions in multilayer silicene. *Appl Phys Lett* 102:163106.
35. De Padova P, et al. (2013) The quasiparticle band dispersion in epitaxial multilayer silicene. *J Phys Condens Matter* 25:382202.
36. Chen L, et al. (2012) Evidence for Dirac fermions in a honeycomb lattice based on silicon. *Phys Rev Lett* 109:056804.
37. Feng B, et al. (2013) Observation of Dirac cone warping and chirality effects in silicene. *ACS Nano* 7:9049–9054.
38. Lin C-L, et al. (2013) Substrate-induced symmetry breaking in silicene. *Phys Rev Lett* 110:076801.
39. Guo Z-X, Furuya S, Iwata J-i, Oshiyama A (2013) Absence and presence of Dirac electrons in silicene on substrates. *Phys Rev B* 87:235435.
40. Cahangirov S, et al. (2013) Electronic structure of silicene on Ag(111): Strong hybridization effects. *Phys Rev B* 88:035432.
41. Wang Y-P, Cheng H-P (2013) Absence of a Dirac cone in silicene on Ag(111): First-principles density functional calculations with a modified effective band structure technique. *Phys Rev B* 87:245430.
42. Quhe R, et al. (2014) Does the Dirac cone exist in silicene on metal substrates? *Sci Rep* 4:5476.
43. Chen MX, Weinert M (2014) Revealing the substrate origin of the linear dispersion of silicene/Ag(111). *Nano Lett* 14:5189–5193.
44. Liu GD, et al. (2008) Development of a vacuum ultraviolet laser-based angle-resolved photoemission system with a superhigh energy resolution better than 1 meV. *Rev Sci Instrum* 79:023105.
45. Reinert F, Nicolay G, Schmidt S, Ehm D, Hüfner S (2001) Direct measurements of the L-gap surface states on the (111) surface of noble metals by photoelectron spectroscopy. *Phys Rev B* 63:115415.
46. Zhou SY, et al. (2007) Substrate-induced bandgap opening in epitaxial graphene. *Nat Mater* 6:770–775.
47. Rotenberg E, et al. (2008) Origin of the energy bandgap in epitaxial graphene. *Nat Mater* 7:258–259.
48. Satta M, Colonna S, Flammini R, Cricenti A, Ronci F (2015) Silicon surface reactivity at the Ag(111) surface. *Phys Rev Lett* 115:026102.
49. Feng Y, et al. (2014) Observation of a flat band in silicene. *Chin Phys Lett* 31:127303.
50. Schneider CM, et al. (2012) Expanding the view into complex material systems: From micro-ARPES to nanoscale HAXPES. *J Electron Spectros Relat Phenom* 185:330–339.
51. Perdew JP, Burke K, Ernzerhof M (1996) Generalized gradient approximation made simple. *Phys Rev Lett* 77:3865–3868.
52. Hohenberg P, Kohn W (1964) Inhomogeneous electron gas. *Phys Rev* 136:B864–B871.
53. Kohn W, Sham LJ (1965) Self-consistent equations including exchange and correlation effects. *Phys Rev* 140:A1133–A1138.
54. Blöchl PE (1994) Self-consistent equations including exchange and correlation effects. *Phys Rev B* 50:17953.
55. Kresse G, Joubert D (1999) From ultrasoft pseudopotentials to the projector augmented-wave method. *Phys Rev B* 59:1758–1775.
56. Kresse G, Hafner J (1993) Ab initio molecular dynamics for liquid metals. *Phys Rev B* 47:558–561.
57. Kresse G, Furthmuller J (1996) Efficient iterative schemes for ab initio total-energy calculations using a plane-wave basis set. *Phys Rev B Condens Matter* 54:11169–11186.
58. Monkhorst HJ, Pack JD (1976) Special points for Brillouin-zone integrations. *Phys Rev B* 13:5188.